

A Quarter Century of Baker-Map Exploration

Wm.G. Hoover¹, C.G. Hoover²

*Ruby Valley Research Institute
601 Highway Contract 60
Ruby Valley, Nevada 89833, USA*

¹*E-mail: hooverwilliam@yahoo.com*

²*E-mail: hoover1carol@yahoo.com*

Received: 9 April 2023; revised: 17 April 2023; accepted: 18 April 2023; published online: 17 May 2023

Abstract: 25 years ago the June 1998 Focus Issue of “Chaos” described the proceedings of a workshop meeting held in Budapest and called “Chaos and Irreversibility”, by the organizers, T. Tél, P. Gaspard, and G. Nicolis. These editors organized the meeting and the proceedings’ issue. They emphasized the importance of fractal structures and Lyapunov instability to modelling nonequilibrium steady states. Several papers concerning maps were presented. Ronald Fox considered the entropy of the incompressible Baker Map $B(x, y)$, shown here in Fig. 1. He found that the limiting probability density after many applications of the map is ambiguous, depending upon the way the limit is approached. Harald Posch and Bill Hoover considered a time-reversible version of a compressible Baker Map, with the compressibility modelling thermostatting. Now, 25 years later, we have uncovered a similar ambiguity, with the information dimension of the probability density giving one value from pointwise averaging and a different one with areawise averaging. Goldstein, Lebowitz, and Sinai appear to consider similar ambiguities. Tasaki, Gilbert, and Dorfman note that the Baker Map probability density is singular everywhere, though integrable over the fractal y coordinate. Breymann, Tél, and Vollmer considered the concatenation of Baker Maps into MultiBaker Maps, as a step toward measuring spatial transport with dynamical systems. The present authors have worked on Baker Maps ever since the 1997 Budapest meeting described in “Chaos”. This paper provides a number of computational benchmark simulations of “Generalized Baker Maps” (where the compressibility of the Map is varied or “generalized”) as described by Kumičák in 2005.

Key words: random walk, fractal, Baker Map, information dimension, Kaplan-Yorke dimension

I. Numerical Simulations of Many-Body Dynamics

Statistical mechanics, developed in the 19th and early 20th centuries by Boltzmann in Austria, Gibbs in the United States, and Maxwell in England, provides a formalism giving macroscopic thermodynamic properties in terms of microscopic (q, p) phase-space trajectory properties. But the complexity of systems more complicated than the ideal gas or the harmonic crystal prevented much progress on “realistic” many-body problems in particle or astrophysical dynamics. By the mid-20th century computers played a huge role in designing weapons for World War II. Their ability to solve complex problems quickly caught the attention of physicists,

mathematicians, engineers, chemists, . . . , all of whom were stymied by the complexity of their nonlinear equations in many variables. After the war computers could be applied to many of the “hard problems” that had accumulated as fruits of the scientific revolution. Computer simulations of many-body problems were developed at universities and national laboratories worldwide. Straightforward applications of particle mechanics and statistical mechanics stimulated international collaborations long before email could make such cooperation routine.

As a result of 1980s and 1990s workshop and conference meetings in Berlin, Budapest, Gmunden, New Hampshire, Orsay, Warwick, and Zakopane, Bill, with half a dozen

colleagues, developed several one-body toy-model small systems designed to shed light on the simulation of (irreversible) nonequilibrium systems with time-reversible equations of motion [1–5]. Among the research goals of these scientists were the resolutions of two paradoxes which had puzzled Maxwell and Boltzmann and their followers, Loschmidt’s, a consequence of time-reversible motion equations:

“How can time-reversible motion equations simulate irreversible processes?”

and Zermélo’s, a consequence of the Poincaré recurrence of any dynamical Hamiltonian state in a bounded portion of its (q, p) phase space:

“How can entropy only increase if the initial state will inevitably recur?”

Applications of two computational innovations combined to provide resolutions of these paradoxes. In the mid-1980s Shuichi Nosé developed a revolutionary variant of Hamiltonian dynamics [6, 7]. He introduced a control variable, his “time-scaling variable”, influencing the kinetic temperature. This modified dynamics, still time-reversible, enabled the simulation of systems at a specified kinetic temperature rather than at constant energy. This work was improved and simplified by Bill [8, 9] as a result of conversations he and Shuichi had near the Notre Dame Cathedral in 1984. They had met by chance at a train station in Paris, a few days prior to a CECAM workshop in Orsay. By 1986 Nosé-Hoover dynamics was generalized to the simulation of nonequilibrium steady states. Bill, along with half a dozen colleagues, developed three toy-model problems illustrating applications of the new mechanics’ temperature control to three nonequilibrium systems: the Galton Board [2], the Galton Staircase [1, 3], and, a decade later, the Conducting Oscillator [5]. The three problem types all exhibited irreversible chaotic solutions (exponentially sensitive to perturbations) despite the deterministic time-reversibility of the dynamics. (1) The Galton Board problem follows the field-driven isokinetic motion of a hard disk through a fixed lattice of identical hard-disk scatterers. The resulting phase-space distribution is fractal [2, 10], a distribution with a nonintegral topological dimensionality. (2) The Galton Staircase problem likewise follows a thermostatted field-driven motion, but of a unit-mass point with momentum p in a sinusoidal potential. The equations of motion for the Galton Staircase are

$$\dot{q} = p; \quad \dot{p} = F - \sin(q) - \zeta p; \quad \dot{\zeta} = p^2 - T.$$

(3) The Conducting Oscillator problem [5] simulates the motion of a heat-conducting harmonic oscillator thermostatted with a coordinate-dependent temperature $T(q) = 1 + \epsilon \tanh(q)$.

All three of these Nosé-Hoover modifications of Hamiltonian flows can generate fractal distributions and do also obey the phase-space continuity equation expressing the co-moving conservation of probability $f dq dp d\zeta = f \otimes$. Here f is the probability density and \otimes is an infinitesimal phase volume element:

$$\begin{aligned} (\dot{f}/f) &= -(\dot{\otimes}/\otimes) = -[(\partial\dot{q}/\partial q) + (\partial\dot{p}/\partial p) + (\partial\dot{\zeta}/\partial\zeta)] = \\ &= \zeta = (\dot{S}/k). \end{aligned}$$

Gibbs’ and Boltzmann’s identification of entropy with $\langle -k \ln f \rangle$ identifies the Nosé-Hoover friction coefficient ζ with entropy production \dot{S} . This is a useful result in interpreting nonequilibrium simulations including the instantaneous heat transfer to the external heat baths represented by the temperature-control variable $\zeta = (\dot{S}/k)$. Here k is Boltzmann’s constant. For convenience we usually choose it equal to unity.

In these three deterministic time-reversible models thermostating is implemented by integral feedback forces imposing a given kinetic temperature $\langle p^2 \rangle$, with control forces $\{-\zeta p\}$ linear in the moving particle’s momentum p . These model systems are sufficiently simple that their phase-space distributions can be analyzed precisely [10, 11] to determine the power-law variation of phase-space bin probabilities $P(\delta)$ with bin size δ . The resulting box-counting and correlation dimensionalities of the fractal distributions describe the scaling of the zeroth and second powers of bin probabilities $\{P\}$. The information dimension is logarithmic. It corresponds to $\langle \ln(P) \rangle / \ln(\delta)$, giving the powerlaw variation of the density of points with respect to the bin size. Information dimension arises naturally in analyzing thermostatted mechanics and is the focus of our attention here. One-, two-, and three-dimensional objects in a three-dimensional space have probabilities varying as the first, second, and third powers of the bin size δ . Accordingly, the definition of the information dimension, $D_I = \langle \ln(P) \rangle / \ln(\delta)$, is a natural generalization of dimension from the integers 1, 2, 3 to a continuously variable “fractal” value. In the special toy-model cases stud-

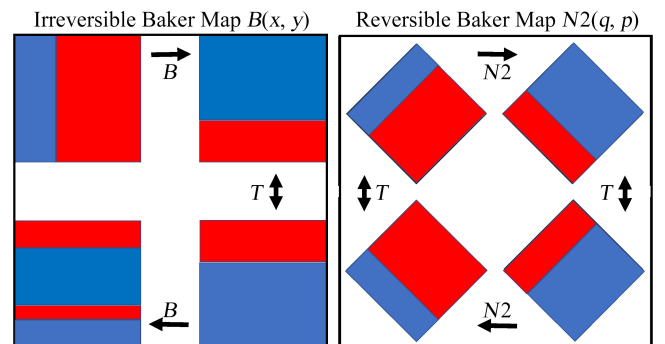


Fig. 1. The two-panel $B(x, y)$ (at left) and $N2(q, p)$ (at right) versions of the compressible nonequilibrium Baker Map. For convenience the mapping is illustrated in the unit square, $0 < x, y < 1$ at the left and in a 2×2 diamond at the right with $-\sqrt{2} < q, p < +\sqrt{2}$. In both cases the mapping T , not to be confused with temperature, changes the sign of the vertical coordinate, $T(\pm x, \pm y) = (\pm x, \mp y)$ at the left and $T(\pm q, \pm p) = (\pm q, \mp p)$ at the right. Note that the bottom leftmost configuration differs from a time-reversed image of the top left image, showing that map B is not time-reversible. The 45 degree rotated mapping $N2$ at the right satisfies time reversibility $N2 \cdot T \cdot N2 \cdot T(q, p) = I(q, p) = (q, p)$, and so is a more faithful analog of time-reversible classical mechanics. I is the identity mapping

ied in the 1980s and 1990s most distributions turned out to have anisotropic fractional rather than integral dimensionalities, characteristic of nonequilibrium steady states. Under some conditions one-dimensional dissipative limit cycles resulted [5].

II. Time-Reversible Chaos and the Two-Dimensional Baker Map

Solutions of Hamilton’s or Lagrange’s or Newton’s or Nosé-Hoover’s motion equations are all “time-reversible”. A transparent example is the formulation and solution of the one-dimensional harmonic oscillator problem with unit mass and force constant;

$$\begin{aligned} \dot{q} &= p ; \dot{p} = -q \rightarrow \ddot{q} = -q \text{ [Hamiltonian Oscillator] ;} \\ \ddot{x} &= -x(t) \text{ [Newtonian Oscillator] ;} \\ \ddot{x} &= -x(t) - \zeta \dot{x} ; \dot{\zeta} = \dot{x}^2 - T \text{ [Nosé-Hoover Oscillator] .} \end{aligned}$$

Given initial values of the coordinate, x or q , at the current and previous times, $x(t)$ and $x(t - dt)$, one can integrate either forward or backward, extending the coordinates’ time series as far into the future or past as desired. Time reversibility can be confirmed by integrating for one timestep, changing the sign of dt and integrating (backward in time) for one step, and then again changing the time, returning to the initial values of $x(t)$, $\dot{x}(t)$, $\zeta(t)$ or $(q(t), p(t))$. Adding a Nosé-Hoover thermostating force $-\zeta p$ the dynamics retains time-reversibility so long as ζ changes sign in the reversed motion, behaving like a momentum variable [9].

Studies of chaotic flows (with the exponential growth of small perturbations) require at least three dynamical variables. In a bounded region of one-or-two-dimensional space a deterministic trajectory must eventually either stop or trace out a periodic orbit, and so cannot be chaotic. Graphics can be simplified by considering projections or cross-sections of three-dimensional flows. A little reflection shows that cross-sections of flows are equivalent to *maps*, with deterministic finite jumps from one phase-space point to another

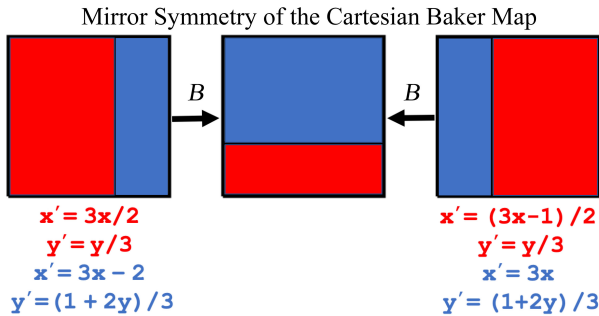


Fig. 2. The mirror symmetry of the Baker map implies that the dividing line between the two mappings, contracting the red region and expanding the blue, can be located at $x = 1/3$ (at the right, above) or $x = 2/3$ (at the left). The analytic forms of the red and blue mappings are colored accordingly. The red mappings halve the area while the blue mappings expand it, in both cases by a factor of two. The primed coordinates describe coordinates in the central unit square

rather than a smooth continuous flow. Let us consider the reversibility of maps. Textbook maps were typically both dissipative and irreversible in 1987 [1]. At that time Bill had no idea that maps could be time-reversible. He wrote [1]:

“The mathematical structures of dissipative maps and the hydrodynamic equations are inherently irreversible. The Nosé-Newton equations are different: They are time-reversible.”

III. Generating Time-Reversible Baker Maps

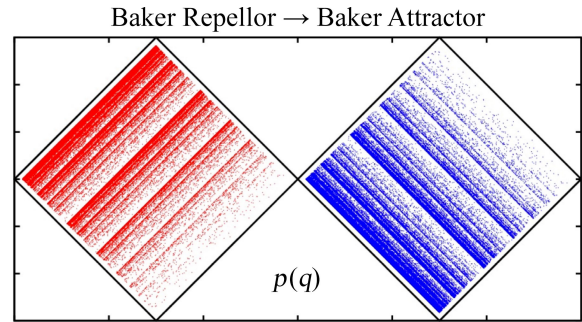


Fig. 3. 100,000 iterations of the inverse $N2^{-1}$ of the nonequilibrium Baker Map $N2(q, p)$ generate the fractal repellor (red, at the left). Changing the sign of the vertical “momentum” p generates the fractal attractor (blue, at the right) from the repellor. Pointwise analyses of either fractal with trillions of iterations suggest an information dimension $D_I = 1.7415$. The mappings shown here were achieved “pointwise”, by repeated mappings of a single point. The limiting extrapolated steady-state information dimensions of the two fractals, based on large- n meshes of width $(1/3)^n$, are close to 1.741, as is discussed in the text. The Kaplan-Yorke Lyapunov dimension is significantly smaller, 1.7337 for the two rotated Baker maps. Figs. 4 and 9 illustrate a similar puzzle, where all eight histograms in those two figures have exactly the same information dimensions, 1.78969

If a *time-reversible* map $M(q, p)$ maps a coordinate q and momentum p forward for one step then it must obey the identity $I = M \cdot T \cdot M \cdot T$, where T changes the sign of the momentum p and I is the identity,

$$I(q, p) = (q, p) ; M(q, p) = (q', p') ; T(q, \pm p) = (q, \mp p) .$$

We choose the left-to-right convention, 123... , for the ordering of sequences of mappings. For instance, with M time-reversible, the sequence of four mappings $M \cdot T \cdot M \cdot T$ corresponds first to stepping forward with M , second to shifting into reverse, third to stepping backward with M , and fourth, to changing the direction of motion from reverse to forward, matching the original direction of motion, $M \cdot T \cdot M \cdot T = I$.

Reversibility can be implemented by considering the rotational modification $N2$ of the Baker’s Map B , shown at the right in Fig. 1. This modification clears the way for area changes corresponding to the production of Boltzmann-Gibbs’ entropy. The two-panel Baker map $N2$ (at the left)

doubles the size of an area element $dxdy$ in the blue region at upper left and halves that of an element from the larger red region. The two mappings (one for red points and one for blue) are linear, with the “new” coordinate or momentum of the form $A + Bq + Cp$. The constants (A, B, C) can be identified relatively easily from the mappings of the vertices of like-colored regions. See the example equations in Fig. 2, which illustrates a useful mirror symmetry of the Cartesian (x, y) Baker Map.

The resulting mappings for the two-panel Baker maps can be expressed as follows: in conventional Cartesian coordinates, with $0 < x, y < 1$ the rightmost Baker map B in Fig. 2 describes the mapping of the blue elements as follows:

$$x < (1/3) \longrightarrow x' = 3x; y' = (1+2y)/3 \text{ [Blue Mapping]} .$$

The red elements in the rightmost B mapping likewise follow linear equations:

$$x > (1/3) \longrightarrow x' = (3x-1)/2; y' = y/3 \text{ [Red Mapping]} .$$

To check the reversibility of these maps simply apply the combination $B \cdot T \cdot B \cdot T$ to the vertices and check to see whether or not the original points are recovered. Because the combination mapping $B \cdot T \cdot B$ produces four parallel horizontal strips rather than two vertical strips at the lower left of Fig. 1 the Cartesian Baker Map B (at top left) is *not* time-reversible.

By analogy with flows a map M is said to be time-reversible when it can be reversed by a three-step process: (1) changing the signs of the momentum-like variables, (2) propagating all the variables one (“backward”) iteration, and then changing the signs of the momenta once more, so that the inverse of the map M is given by $M^{-1} = T \cdot M \cdot T$. In ordinary Hamiltonian mechanics the T mapping simply maps $(\pm q, \pm p) \rightarrow (\pm q, \mp p)$. Bill’s conversations with Bill Vance and Joel Keizer during Vance’s graduate work at the University of California’s Davis campus led us to a nonequilibrium *rotated* version of the Baker Map B which we call $N2$, N for “Nonequilibrium”, with “2” for two panels. This Map’s domain is the diamond-shaped region, centered on $(q, p) = (0, 0)$ and shown at the right of Fig. 1 and again in Fig. 3. Now imagine that the map $N2$ is applied to a representative input point (q, p) . This operation produces the next point (q', p') .

Our rotated nonequilibrium Map, $N2(q, p) \rightarrow (q', p')$ has the following analytic form: For (blue in Fig. 1) twofold expansion, $q < p - \sqrt{2/9}$:

$$\begin{aligned} q' &= (11q/6) - (7p/6) + \sqrt{49/18}; \\ p' &= (11p/6) - (7q/6) - \sqrt{25/18}. \end{aligned}$$

For (red in Fig. 1) twofold contraction, $q > p - \sqrt{2/9}$:

$$\begin{aligned} q' &= (11q/12) - (7p/12) + \sqrt{49/72}; \\ p' &= (11p/12) - (7q/12) - \sqrt{1/72}. \end{aligned}$$

Fig. 3 shows the resulting concentration of probability into bands parallel to the attractor’s bottom left and the repeller’s upper left edges of their diamond-shaped domains.

Although the algebra is more cumbersome we have chosen to use the rotated $N2(q, p)$ version of this map, centered on the origin and confined to a diamond-shaped region of sidelength 2, as shown at the right in Figs. 1 and 3. We regard the horizontal q variable as a coordinate and the vertical p variable as a momentum. Figs. 1 and 3 illustrate the time-reversibility of the (q, p) map. This similarity to nonequilibrium molecular dynamics, along with the square roots generating the 45° rotation, are twin advantages of this nonequilibrium diamond-shaped map $N2$. The square roots eliminate most of the artificial periodic orbits resulting from finite computer precision. Beginning at the center point of the Cartesian rational-number square map, $(x, y) = (0.5, 0.5)$, leads to a periodic orbit of just 3095 single-precision iterations. Starting instead at the equivalent central point of the irrational-numbered diamond map, $(q, p) = (0.0, 0.0)$, leads to a single-precision periodic orbit of 1 124 068 iterations. With double-precision arithmetic the orbits are much longer. 10^{12} such (x, y) iterations from the same initial condition gave no repeated points. Let us next consider an approximate theoretical approach to analyzing the Baker fractal followed by two computational algorithms. We will find several interesting surprises in so doing. For a striking example see Figs. 4 and 9 which display eight different histograms for two distinct mappings, $N2$ and $N3$, with all eight giving *exactly the same* areawise information dimension, 0.78969.

IV. Kaplan and Yorke’s Conjectured Dimension

It has been argued [11] that the fractal information dimension is best suited to characterizing fractal distributions of points because it is uniquely insensitive to changes of variables. For that reason Kaplan and Yorke’s conjectured relation [12, 13] between the Lyapunov spectrum $\{\lambda_i\}$ and the information dimension, $D_{KY} = 1 - (\lambda_1/\lambda_2) \stackrel{?}{=} D_I$ in this case, is of special interest. How does this relationship arise? We quote from page 169 of Tamás Tél’s and Márton Gruiž’ excellent book [12], *Chaotic Dynamics*:

“Both the information dimension and the average Lyapunov exponents are determined by the natural distribution. We can therefore expect to find an explicit relation between them. This rule, called the Kaplan-Yorke relation, is valid for chaotic attractors of general two-dimensional invertible maps, and can be obtained from a simple argument.”

This is followed by two pages of informal text ending up with the “valid” rule above. Because the “rule” is violated by the simple $N2$ map, with

$$\begin{aligned} D_I &= 0.7415 \text{ [from simulations]}; \\ D_{KY} &= 0.7337 \text{ [from Lyapunov Exponents]}, \end{aligned}$$

the reasoning supporting the conjecture is obscure. Because the Baker Map is linear one might expect that it would likely

follow the conjectured relation. Kaplan and Yorke suggested that a linear interpolation formula between the number of terms in the *last positive sum* of exponents, starting with the largest, λ_1 , and the number of terms in the next sum (*the first negative sum*, with one term in addition to those in the previous sum), would be a useful estimate for the information dimension [13]. In fact they cite many a case, including theoretical work carried out by L.S. Young, for which their conjectured estimate is exactly correct.

The red portion of the compressible Baker Map of B in Fig. 1 represents the $(2/3)$ of the measure that stretches horizontally by a factor $(3/2)$ while the blue portion represents that $(1/3)$ of the measure that stretches by a factor of 3 in the same direction, horizontally. As a result the longtime stretching rate per iteration is

$$\lambda_1 = \frac{2}{3} \ln\left(\frac{3}{2}\right) + \frac{1}{3} \ln(3) = \frac{1}{3} \ln\left(\frac{27}{4}\right) = 0.63651 .$$

Likewise $(2/3)$ of the measure shrinks vertically by a factor 3 as does $(1/3)$ by a factor $(2/3)$ so that

$$\lambda_2 = \frac{2}{3} \ln\left(\frac{1}{3}\right) + \frac{1}{3} \ln\left(\frac{2}{3}\right) = \frac{1}{3} \ln\left(\frac{2}{27}\right) = -0.86756 .$$

The linear interpolation between the single-term “positive sum”, 0.63651, and the two-term sum, $0.63651 - 0.86756 = -0.23105$, gives an interpolated “number of terms for a sum of zero”, $1 + (0.63651/0.86756) = 1.73368$. This dimension, sometimes called the “Lyapunov dimension” is the Kaplan-Yorke dimension D_{KY} .

In their 1998 paper [4], presented at the 1997 Budapest Meeting on Chaos and Irreversibility [14], Bill and Harald Posch introduced the two-panel nonequilibrium $N2$ Baker map. The model stimulated more work at the meeting [15] and subsequently [16]. In 2005 Kumičák wrote a very readable paper [16] emphasizing the connection of “Generalized Baker maps” to the phase-space contractability (to fractals) providing improved understanding of the emergence of the Second Law of Thermodynamics for such models. Kumičák characterized his generalized maps with the variable w . The fraction of a unit-square mapping occupied by the narrowest strip, is $1/w$, $1/3$ for the $N2$ mapping of Fig. 1 and 2. Like Hoover and Posch, he assumed that Kaplan and Yorke’s conjecture for the information dimension was true. For the nonequilibrium w values of 3, 4, and 5 he quotes information dimensions 1.734, 1.506, and 1.376, as well as a formula for all the generalized Baker Maps. A decade later, with Florian Grond [17], we checked this Kaplan-Yorke assumption for a four-dimensional flow, as opposed to a map. We chose the four-dimensional chaotic oscillator flow,

$$\{ \ddot{q} = -q - \zeta \dot{q} - \xi \dot{q}^3 ; \dot{\zeta} = \dot{q}^2 - T ; \dot{\xi} = \dot{q}^4 - 3\dot{q}^2 T \} \longrightarrow \longrightarrow D_{KY} = 2.80 > D_I = 2.56 .$$

and soon discovered that the conjecture fails in that case. For that four-dimensional chaotic problem, with a relatively strong temperature gradient, $T = 1 + \tanh(q)$, the interpolated Lyapunov sum, between those for two and for three exponents, $\lambda_1 + \lambda_2 + 0.80\lambda_3$, vanishes. The consequent Kaplan-Yorke dimension, 2.80, differs by about ten percent from the

bin-based dimensionality of 2.56. These results, along with those that follow here leave the status of the conjecture perplexing. It would be useful to have a clear informal description of maps for which the conjecture is known to be true accompanied by an illustrative list of situations where it fails.

V. Areawise and Pointwise Information Dimensions

$N2$ Probability Densities for 1, 2, 3, 4 Iterations

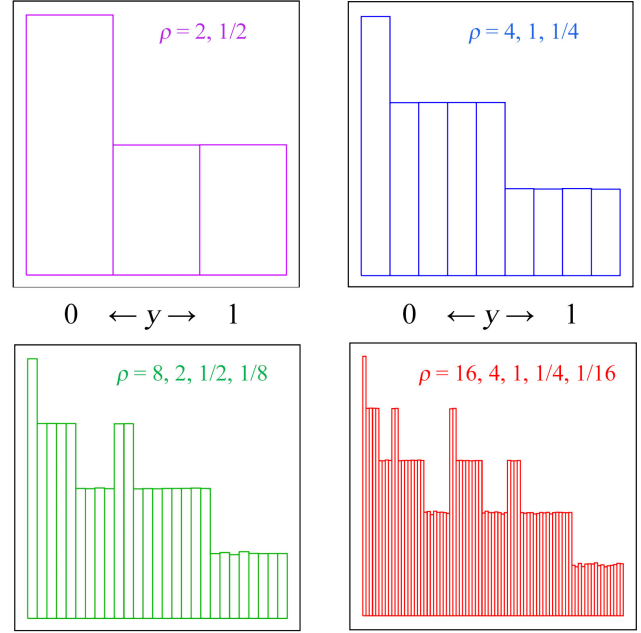


Fig. 4. Histograms of the (base-4 logarithm of) probability density $\rho(y)$ for 1, 2, 3, and 4 areawise iterations of the y component of the Baker Map B . Notice that the number of bins at each level of probability is the product of a binomial coefficient and a power of two, in the red case $1 \times 1, 4 \times 2, 6 \times 4, 4 \times 8, 1 \times 16$, for a total of $3^4 = 81$ bins of width $1/81$. Notice here that the leftmost third of the unit interval, with summed-up probability $2/3$, is reproduced as a scale model (with the same information dimensionality) in the rightmost two thirds of the interval, with probability $1/3$. The information dimensions of all these iterates, $D_I = \sum (P \ln P) / \ln(\delta) = 0.78969$ are identical. This scale-model result differs from both the Kaplan-Yorke value of 0.7337 and the extrapolated pointwise value 0.7415 , based on mesh sizes of $(1/3)^n$ and illustrated in Fig. 5. The histograms were constructed by binning (in 3, 9, 27, and 81 bins) the results of 1, 2, 3, and 4 iterations of 100,000 equally spaced initial values on the interval $0 < y < 1$. Each iteration reproduces the previous cumulative densities, but with threefold finer structure. These previous densities likewise agree with those generated from another map, $N3$, illustrated in Figs. 8 and 9

Numerical analyses of the fractal structures generated by the compressible Cartesian version of the $N2$ Baker Map reveals that there is *no fractal structure* in the x direction. Only the y coordinate reveals fractal structure. See again the rotated maps’ fractals in Fig. 3. This suggests two computational approaches to determining the information dimension associated with the y direction in map B or the $q = p$ direction in map $N2$:

1. Propagating *area* mappings, starting with a homogeneous square-lattice covering of the initial unit square or the rotated 2×2 diamond-shaped domain of Fig. 1;
2. Accumulating bin occupancies of *points*, with as many as trillions of iterations generating a long sequence of *points* starting from an arbitrary initial point.

Approaches (1) and (2), areawise and pointwise, respectively appear to be equally legitimate routes to information dimension. It was a surprise to us to find that the two don't agree although both these approaches do reach well-defined limits. Another approach, (3), which we term "stochastic", adopts random numbers for successive values of x (the Lyapunov-unstable nonfractal expanding direction) rather than using the more time-consuming analytic $N/2$ mapping. With random numbers $\{0 < r < 1\}$ the third approach is simply a confined random walk ($0 < y < 1$) with red-region "up" steps, to $(1 + 2y)/3$ one-third of the time and "down" steps to $(y/3)$ two-thirds of the time. The programming of a single stochastic step requires one or two calls to a random-number generator (for which we use a standard random-number FORTRAN subroutine). A sample program is included in Fig. 12. Note the underscore, not a hyphen, in this four-line snippet:

```
call random_number(r)
if(r.lt.1/3) ynew = (1+2y)/3
if(r.gt.1/3) ynew = (0+ y)/3
call random_number(x)
```

We have already seen, in Fig. 4, that the areawise mapping used to generate the histograms, simply repeats the single-iteration three-bin information dimension, 0.78969. The pointwise mapping is simpler. It is only limited by available computer time. A personal computer is quite capable of trillions of pointwise iterations. A billion pointwise iterations take about a minute of computer time. Using double-precision and an initial point $(x, y) = (0.5, 0.5) \longleftrightarrow (q, p) = (0, 0)$, the two algorithms, pointwise and stochastic agree, as expected, to four-figure accuracy, with the following division of the unit interval into three strips:

$$(0 < y < 1/3), (1/3 < y < 2/3), (2/3 < y < 1) .$$

For a total of one billion points the three-strip bin probabilities (summing to unity) and the corresponding information dimensions for the two algorithms are in overall agreement:

$$\text{pointwise : } 0.666\ 681\ 049 + 0.295\ 151\ 739 + \\ + 0.038\ 167\ 212 \rightarrow D = 0.6873;$$

$$\text{stochastic : } 0.666\ 631\ 518 + 0.295\ 178\ 423 + \\ + 0.038\ 190\ 059 \rightarrow D = 0.6874.$$

The close agreement suggests that areawise mapping is an outlier and recommends the adoption of pointwise distributions. We consider some interesting details of that approach next.

Compressible $N/2$ Baker Map "Information Dimension"

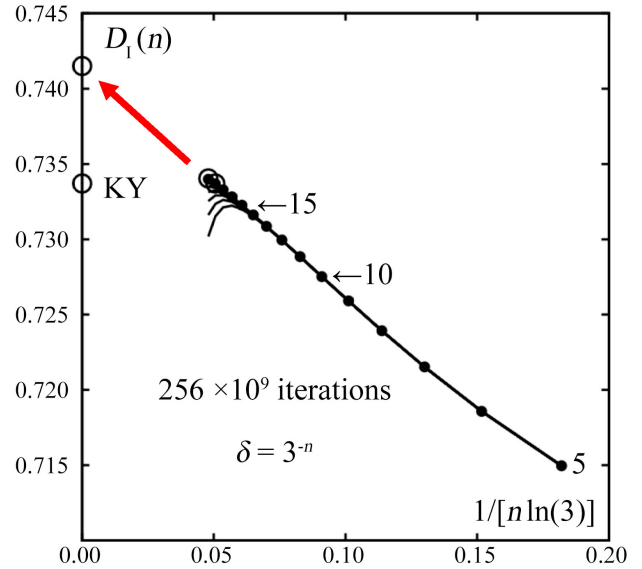


Fig. 5. Stationary estimates of D_I for the confined-random-walk model of the Baker Map with results for $3^{5,10,15}$ equal bins emphasized. We saw above that the two values shown at the zero bin-size limit ($\delta \rightarrow 0$) correspond to the Kaplan-Yorke dimension, 0.7337, and a plausible extrapolation of trillion-iteration computations with as many as 3^{19} bins, 0.7415. Note the qualitative difference of the mesh dependence (the slope is uniformly negative here for $\delta = 3^{-n}$) compared to those shown in the next two Figs. 6 and 7 for 4^{-n} , 5^{-n} , 6^{-n} , and 7^{-n} . Two data here are from relatively long runs. The two open circles at $n = 18$ and 19 correspond to 1.024×10^{12} iterations. The smaller dots correspond to sequences of 256 billion points

It is easy to verify that the one-dimensional and two-dimensional pointwise information dimensions agree with one another for readily convergent simulations with moderate bin sizes, $\delta = 3^{-10}$ or 3^{-15} . These results also agree very well with stochastic-map values corresponding to the rightmost mapping of Fig. 2 where x represents a random number from the interval ($0 < x < 1$).

$$x < (1/3) \rightarrow y' = (1 + 2y)/3 ; x > (1/3) \rightarrow y' = (y/3) .$$

For a fixed choice of $\delta_y = (1/3)^n$ the three approaches, as shown above for a billion points, agree to five-figure accuracy, supporting the use of the simpler stochastic approach shown in Fig. 5. The data cover the range from $n = 5$ to $n = 19$, approaching D_I from below, eventually reaching a straight line with a well-defined limit 0.7415. It is straightforward to write a supporting random-walk computer program distributing many successive points over 3^n bins of width $(1/3)^n$. Figs. 5–7 show the results of distributing up to a trillion iterations over as many as $7^{11} \simeq 2 \times 10^9$ square bins.

A one-dimensional area mapping of the Baker map using a uniform distribution of "many" points (millions or billions) on the interval ($0 < y < 1$) puts $2/3$ of them into the left-hand interval of width $\delta = 1/3$. The remaining $1/3$ of this singly-mapped measure is mapped uniformly into the two

remaining bins, center and right, of combined length $2/3$. Fig. 4 illustrates the iterated operation of the compressible Baker Map for 1, 2, 3, and 4 iterations applied to an initially uniform distribution of 100000 points. For simplicity here we have projected the result of the mapping onto the unit interval in y rather than the 2×2 diamond or unit square. Propagating the singly-mapped measure results in measures of $(2/3)$ and $(1/6)$ and $(1/6)$ in the three equal-width bins, and so to an approximate single iteration information dimension after a single iteration of many uniformly-dense points gives

$$D_I(1) = \langle P \rangle / \ln(\delta) = \frac{[\frac{2}{3} \ln(\frac{2}{3}) + \frac{1}{6} \ln(\frac{1}{6}) + \frac{1}{6} \ln(\frac{1}{6})]}{\ln(\frac{1}{3})} = 0.78969 .$$

Here $\delta = 1/3$ is the bin size and the $\{ P \}$ are the probabilities, $(2/3)$ and $(1/6)$, of the three bins. The nine-bin area-wise information dimension follows similarly with the leftmost bin probability of $(4/9)$ followed by four bins with probabilities $(1/9)$ and four more with probabilities $(1/36)$. Summing the 9 or 27 or 81 $P \times \ln(P)$ terms and dividing by $\ln(1/9) \dots \ln(81)$ gives *exactly the same* dimensionality as before, $D_I(2) = 0.78969$. Likewise from the histogram data of Fig. 4 we find $D_I(3) = D_I(4) = 0.78969$.

In summary, we have three distinct estimates for the information dimension of the confined random-walk, 0.7337, 0.741₅, and 0.7897, corresponding to three distinct estimates for the two-dimensional maps B and $N2$, 1.7337, 1.741₅, and 1.7897.

Although initially it is a surprise to find that the same information dimension results for 2 or 3 or 4 or ... areawise iterations, that result is fully consistent with, and implied by, the scale-model nature of the distribution, as shown in Fig. 4. Iterating a uniform coverage of the unit square or diamond

suggests that the information dimension of the Baker maps' history is 1.78969. One would think that the limiting case $\delta \rightarrow 0$ would also result from a long time series generated by pointwise iteration of a single point. However, we saw in Fig. 5 that pointwise iteration suggests a different dimensionality, 1.741₅!

VI. N3, A Well-Behaved Three-Panel Baker Map

Inspection of the $N3$ mapping illustrated by Fig. 8 shows that both the blue and green panels increase in width by a factor 6 and decrease in length by a factor 3, while the red panel, with probability $2/3$, increases by a factor $3/2$ and decreases by a factor 3, giving rise to the Kaplan-Yorke dimension

$$\lambda_1 = +0.867563 ; \lambda_2 = -1.09861231 \rightarrow \rightarrow \lambda_1 + 0.78969\lambda_2 = 0 \rightarrow D_{KY} = +1.789690 ,$$

the same as the information dimensions found with areawise and pointwise analyses. The probabilities associated with $N3$, shown in the histograms of Fig. 9, are identical to those of $N2$, but with a different ordering of the histogram rectangles. Evidently the $N3$ areawise dimensionality, like the $N2$, doesn't change. But unlike $N2$ the $N3$ map does agree with Kaplan-Yorke. In a memoir for Francis Ree [18], Bill chose meshes from $(1/3)^5$ to $(1/3)^{18}$ for a set of 10^{11} iterations of the $N3$ map. Fig. 10 in the Ree memoir appears to be fully consistent with a pointwise estimation $D_I = 0.790$. Within the estimated uncertainty of 0.001 it appears that the $N3$ areawise, pointwise, and Kaplan-Yorke values of the information dimension all agree with one another! This makes the failure of the simpler $N2$ Baker map, with only two linear panels, to provide the same simplicity suggested by Tél and Gruiz [12] a puzzling challenge.

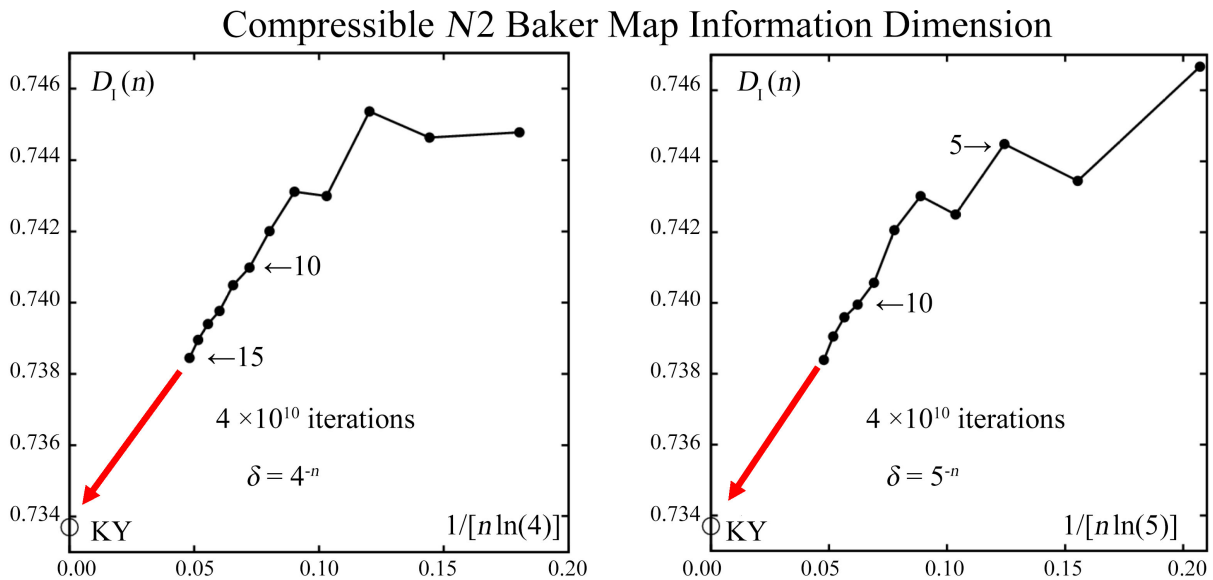


Fig. 6. Stationary estimates for the Baker Map Information Dimension using up to 4^{15} and 5^{13} bins of equal width. These data, based on forty billion iterations of the random walk mapping suggest agreement with the Kaplan-Yorke dimensions of the one-dimensional y version of two-panel Baker Maps, $D_{KY} = 0.7337$

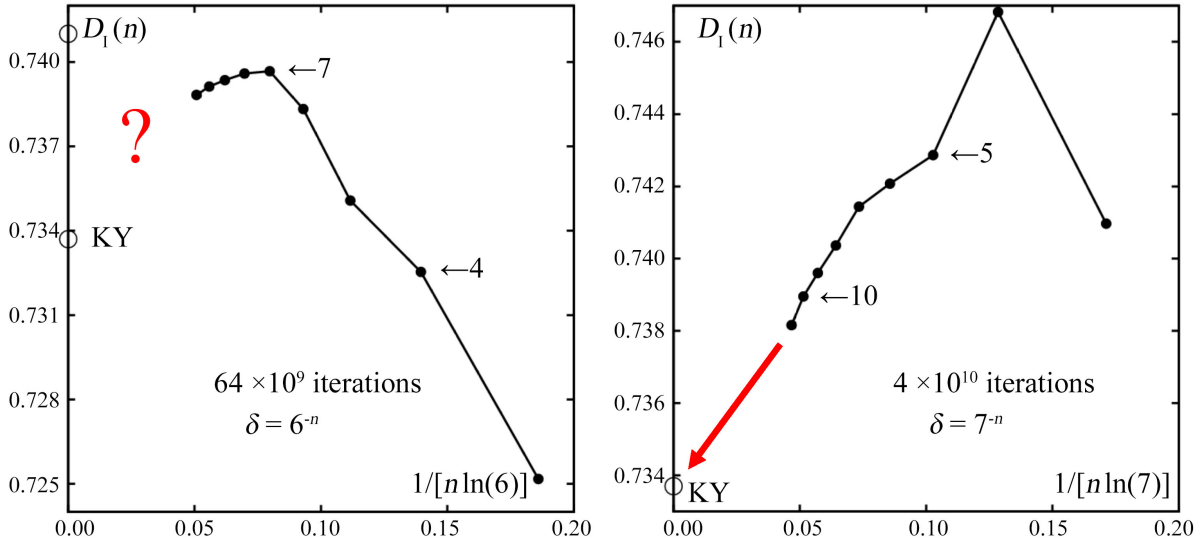
Compressible N_2 Baker Map Information Dimension

Fig. 7. Stationary estimates for the one-dimensional version of the two-panel Baker Maps' Information Dimensions using up to 6^{11} and 7^{11} bins of equal width. These data, like those in Fig. 4, are based on forty billion iterations of the confined random-walk mapping. Both the lower Kaplan-Yorke dimension 0.7337 and the higher estimate 0.741 from page 11 of Ref. 18, based on meshes with up to 3^{19} equal bins, are shown as open circles at the left border of the $\delta = 6^{-n}$ plot

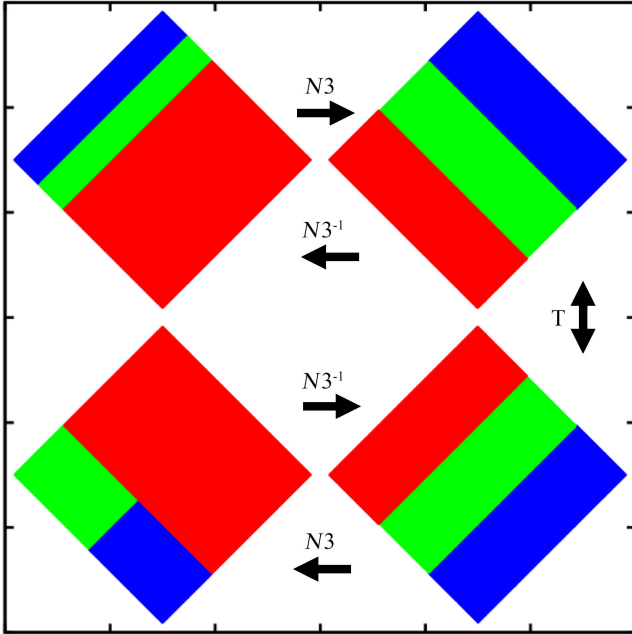
 N_3 Irreversible Baker Map

Fig. 8. The three-panel Baker map N_3 is slightly more complex than the two-panel N_2 map, dividing the upper left blue and green portion in half. Applying the sequence of three maps $N_3 \cdot T \cdot N_3$ shown at the bottom left, is quite different to a mirror image of the original upper left. Evidently the N_3 map is not time-reversible. But both the areawise and the pointwise maps match the Kaplan-Yorke information dimension. Quite unlike the simpler two-panel Baker Map N_2 the three routes to the N_3 information dimension apparently all reach the same value $D_1 = 0.78969$

Like N_2 the three-panel N_3 fractal corresponding to Fig. 8 can be reproduced with calls to a random-number generator. Notice that the generator call includes an underscore, not a hyphen. The simplest program results if the N_3 fractal is generated with the Cartesian y coordinate rather than the rotated q :

```
call random_number(r)
      ynew = (1+y)/3      ! green
if(r.lt.1/6) ynew = (2+y)/3 ! blue
if(r.gt.1/3) ynew = (0+y)/3 ! red
call random_number(xnew)
x = xnew
y = ynew
```

VII. Pointwise Analysis of Generalized Baker Maps

There is a surprising difference between N_2 , with its three information dimensions, and N_3 , with its consistent dimensions, all of them 0.78969 for the stochastic walk and 1.78969 for the (q, p) version of N_3 illustrated in Fig. 8. It is therefore interesting to see how general these disparities are. It is straightforward to consider Kumičák's series of Generalized Baker Maps, where the width of the smaller Baker strip is $1/w$, $1/2$ for the incompressible map, $1/3$ for our N_2 map, and so on. Fig. 10 is the first step in this exploration. It shows pointwise information dimensions for a dozen or so bin sizes for each of the generalized maps within the range $2 < w < 9$.

Each of the filled circles in Fig. 10 shows the finite-bin-size information dimension for two billion points generated with the stochastic analog of the N_2 map of Fig. 1:

```

call random_number(r)
if(r.lt.1/w) ynew = [1+(w-1)y]/w      !   expanding
if(r.gt.1/w) ynew = y/w              !   compressing
call random_number(x)                 !   for the (x,y) version
y = ynew

```

The cut line at $x = (1/w)$ separates the expanding and contracting regions of the unit square or unit interval of y . There is a gradual decrease of $D_{KY}(w)$ as the mesh is refined and it appears that the Kaplan-Yorke dimensions of Fig. 10 are quite close to a straight-line extrapolation of the pointwise data. To check this possibility we invested a bit over a trillion points in a series of four open-circle pointwise measurements with the finest mesh resolution $\delta = 2^{-30}$, a bit less than a billionth. The resulting plot, Fig. 11, does give an excellent straight line. This allows an accurate estimate for the pointwise dimension, $D_1 = 0.512$. This relatively precise result is significantly different to the Kaplan-Yorke $D_{KY} = 0.506$. We conclude that the failure of the Kaplan-Yorke approximation is not limited to $w = 3$ and 4 but likely extends to other maps. It appears that the extrapolation to vanishing δ_y gains both accuracy and precision as the compression and expansion ratios increase from 2 to 3 and beyond.

VIII. Conclusions and Discussion

Relatively simple numerical work, on the order of a few dozen lines of FORTRAN, along with a few hours of laptop time, are enough to characterize our variety of results for D_1 . A sample program, along with its results for the cumulative probabilities for $N2$ and $N3$ appears in Fig. 12. Similar programs take only an hour or so to write. They can seek information dimensions based on (1) iterating areas or (2) generating representative sequences of points. These two different views of fractal structure are analogs of the Liouville and trajectory descriptions of particle mechanics. We think the singular anisotropy is responsible for the ambiguity of the fractals' dimensionalities, and favors the pointwise approach. This corresponds to considering the long-time behavior of a particular system rather than a many-particle ensemble of systems. We found that pointwise analysis with the mesh series $(1/3)^n$ appears to contradict the Kaplan-Yorke dimension while the alternative series $(1/4)^n$, $(1/5)^n$, $(1/7)^n$ appear to support it. The series $(1/6)^n$ is inconclusive.

Though the one-dimensional confined random walk provides a fractal distribution in $\{y\}$, indistinguishable from that for the compressible $N2$ Baker Map, the confined-walk analog lacks the Baker-Map Lyapunov exponents on which the Kaplan-Yorke dimension relies:

$$\lambda_1 = \frac{1}{3} \ln \left(\frac{27}{4} \right); \lambda_2 = \frac{1}{3} \ln \left(\frac{2}{27} \right) \rightarrow D_{KY} = 0.73368.$$

The variety of results obtained here for specific maps, and meshes, time-reversible and not, emphasizes the value of studying particular, as opposed to general, models. There are publications suggesting that the information dimension is particularly robust to changes of variables [11], certainly a desirable property. That work, like Doyné Farmer's [19], assumes that the information dimension can be determined unambiguously, while in fact there appear to be *many* information dimensions, not only pointwise and areawise, but also depending upon the details of the binning and extrapolation to vanishing bin size. It is fortuitous that in some cases (for instance $w = 3$) apparent information dimensions suggest powerlaw extrapolation in powers of $1/\ln(\delta)$. Mathematical results often state that results hold for maps without singular points. Yet the simplest Baker Maps invariably have "cut lines" across which the mapping is discontinuous, causing the nonmathematical specialist alarm.

Returning to the longstanding motivations of Loschmidt's Reversibility Paradox and Zermélo's Recurrence Paradox, compressible maps simplify our understanding of their resolutions, for flows just as well as for maps. Fractal states have zero volume in their embedding spaces. This means that nonequilibrium distributions are typically attractor/repellor pairs. Chaos provides exponentially unstable (and therefore unobservable) repellors and exponentially stable (and therefore inevitable) attractors. Time-reversible maps provide simple fractal examples of Second Law irreversibility despite the paradoxes. Also notable is the quantitative agreement, within Central Limit Theorem fluctuations, of reversible distributions with those generated using stochastic random walks.

Let us summarize the facts that stand out from our work: The simple $N2$ two-panel map, whether one-dimensional, in y , or two-dimensional, in (q, p) , provides three different limiting values of information dimension "areawise", 0.78969 or 1.78969, "pointwise", 0.741₅ or 1.741₅, and Kaplan-Yorke, 0.73368 or 1.73368. The more complex, but still linear, three-panel $N3$ map is not time-reversible but somehow is consistent with $D_1 = 0.78969$ in one dimension and 1.78969 in two dimensions for all three approaches. It appears that there is much work to be accomplished in order to understand the ambiguous nature of what is presumably the simplest and most fundamental of the chaos quantifiers, the information dimension. We encourage the reader to think about such problems and to develop algorithms providing insight into maps as well as flows. In years past we have offered \$1000 Snook Prize awards for interesting CMST papers making progress in various aspects of computational

statistical mechanics. Please address the authors in the event that you would like to contribute research in the area suggested by this paper during the calendar year 2023.

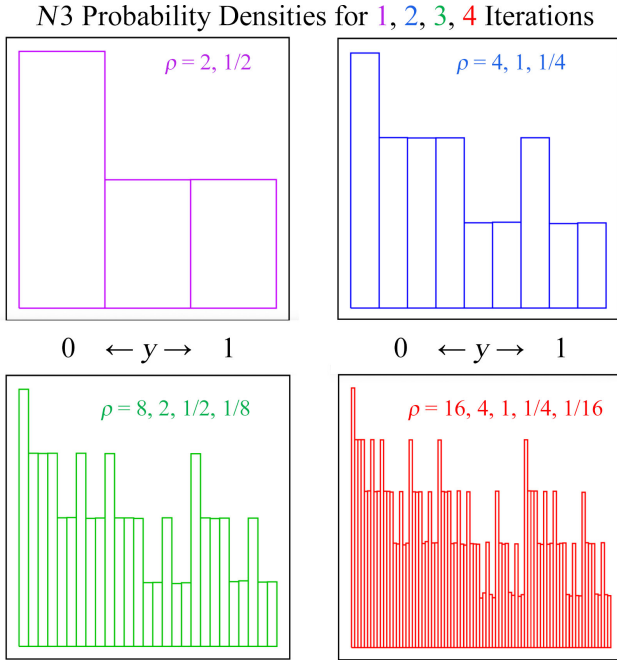


Fig. 9. Histograms of the (base-4 logarithm of) probability density $\rho(y)$ for 1, 2, 3, and 4 areawise iterations of the y component of the nonequilibrium $N3$ Map. Notice that the central and rightmost thirds of each resulting mapping are both perfect scale models (reduced by a factor of four) of the leftmost third. This observation explains the persistence of the three-bin information dimension throughout any number of 3^n iterations with 3^n bins. Notice also that the cumulative distributions (integrals over y) at each iteration stage reproduce the values from the previous iterations, agreeing with those from the histograms in Fig. 4. In both figures the areawise dimension is $D_1 = 0.78969$

IX. An Example FORTRAN Program

We provide a working FORTRAN program which generates a series of y coordinates corresponding to random values of x . The resulting points correspond to the Cartesian form of the Baker Map. The points generate a histogram with one million bins and a total of one million y coordinates. The numbers of bins and coordinates, (NB, NY) are parameters which can be chosen arbitrarily.

Once the histogram has been computed the cumulative sum CUM is calculated and displayed in Fig. 12. Because the histogram is wildly discontinuous the slope of the sum is singular. It is curious that the cumulative sums for the $N2$ and $N3$ maps coincide for bins 3, 9, 27, ..., 3^n , a consequence of both mappings being based on exactly the same sequence of random numbers. The shapes and locations of the two cumulative sums are relatively insensitive to the choices of bin and coordinate numbers.

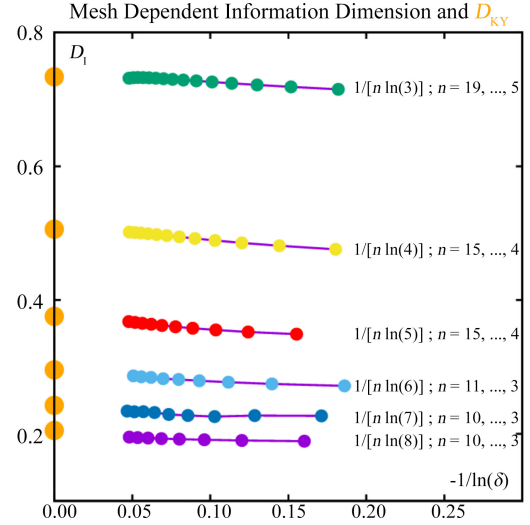


Fig. 10. Dependence of the pointwise information dimension D_1 on the bin size δ for six generalized Baker Maps. The reciprocals of the integers $\{w\}$ from 3 to 8 indicate the fractions of the unit square occupied by the narrower rectangles of the mappings, $1/w$. As an example the $N2$ mapping of Fig. 1 corresponds to the integer 3 with the rectangular areas different by a factor of 2. The points for each mapping give information dimensions for different choices of the bin size, right-to-left from $(1/8)^3$ to $(1/8)^{10}$ for the bottom set of eight purple data points and from $(1/3)^5$ to $(1/3)^{19}$ for the top set of 15 green points. The Kaplan-Yorke approximations are shown as orange filled circles for each of these generalized maps. They are excellent approximations! Each filled circle is the result of two billion steps in a random-walk simulation of the corresponding generalized Baker Map

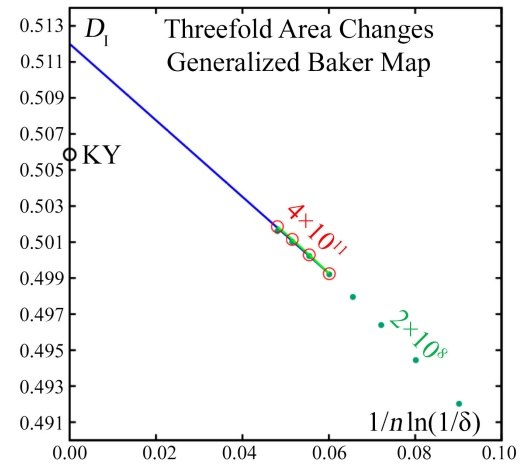


Fig. 11. The information dimension from the definition $\langle \ln(P) \rangle / \ln(\delta)$ is evaluated here for the generalized Baker Map incorporating threefold area changes corresponding to $w = 4$ using from 4^8 to 4^{15} bins with the green points indicating results with two billion iterations and the red open circles indicating 400 billion iterations. Just as in our earlier work with twofold area changes the data clearly approach a linear dependence on the inverse logarithm of the number of bins and show, at $D_1 = 0.512$, a clear deviation from the Kaplan-Yorke prediction $D_{KY} = 0.506$ indicated on the ordinate axis. The deviation, 0.006 here, is a bit smaller than the 0.008 deviation found in Fig. 5 using a like amount of simulation data for the Generalized Baker Mapping with twofold area changes, corresponding to $w = 3$

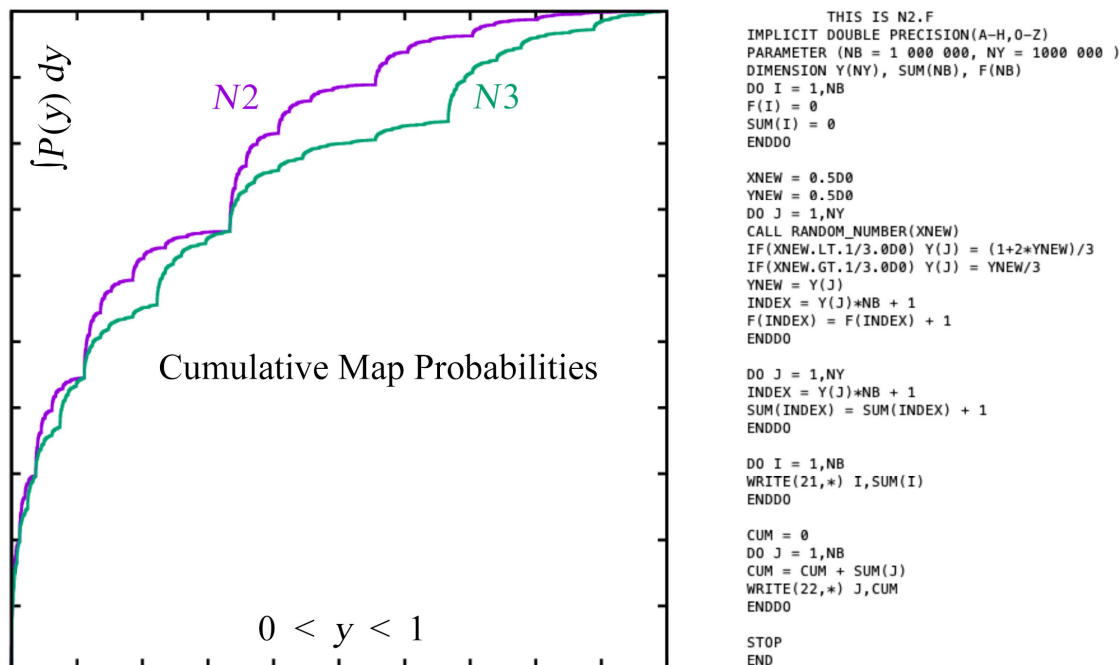


Fig. 12. FORTRAN programming with NB bins and NY y steps in the confined random walk equivalent of the $N2$ mapping. This FORTRAN program uses a standard random-number generator to simulate the binned density and its y integral. A similar program for $N3$ replaces the three lines computing $Y(J)$ and $YNEW$ by the following:

$$Y(J) = (1+YNEW) / 3$$

$$\text{IF}(XNEW.LT.1/6.0d0) \quad Y(J) = (2+YNEW) / 3$$

$$\text{IF}(XNEW.GT.1/3.0d0) \quad Y(J) = (0+YNEW) / 3$$

The curves include one million successive y values distributed into one million bins of width 0.000001. As the numerical calculation in the accompanying FORTRAN requires less than a minute, the rigorous analysis of Ref. 20 (which generates the Kaplan-Yorke dimension) is unnecessary to the visualization of the probabilities. It is interesting that the two curves coincide for numbers of bins which are integral powers of three: 3, 9, 27, ..., 3^n . We don't know whether or not the information dimensions of simple nonequilibrium flows have ambiguities similar to those found here, for maps

Acknowledgment

Carl Dettmann, Thomas Gilbert, Kris Wojciechowski, Tamás Tél, Tim Li, and Ronald Fox kindly provided helpful advice and references. Evidently even the simplest generalized Baker Maps exhibit different areawise and pointwise information dimensions. Surprisingly, it took us 20 years to come to this understanding. We thank our colleagues for their help and again refer the reader to the June 1998 issue of "Chaos" for more details of the work mentioned in the Abstract.

References

- [1] B.L. Holian, W.G. Hoover, H.A. Posch, *Resolution of Loschmidt's Paradox: The Origin of Irreversible Behavior in Reversible Atomistic Dynamics*, Physical Review Letters **59**, 10–13 (1987).
- [2] B. Moran, W.G. Hoover, S. Bestiale, *Diffusion in a Periodic Lorentz Gas*, Journal of Statistical Physics **48**, 709–726 (1987).
- [3] W.G. Hoover, H.A. Posch, B.L. Holian, M.J. Gillan, M. Mareschal, C. Massobrio, *Dissipative Irreversibility from Nosé's Reversible Mechanics*, Molecular Simulation **1**, 79–86 (1987).
- [4] Wm.G. Hoover, H.A. Posch, *Chaos and Irreversibility in Simple Model Systems*, [In:] Proceedings of "Chaos and Irreversibility" at Eötvös University 31 August–6 September (1997), organized by T. Tél, P. Gaspard, G. Nicolis, Chaos **8**, 366–374 (1998).
- [5] H.A. Posch, W.G. Hoover, *Time-Reversible Dissipative Attractors In Three And Four Phase-Space Dimensions*, Physical Review E **55**, 6803–6810 (1997).
- [6] S. Nosé, *A Molecular Dynamics Method for Simulations in the Canonical Ensemble*, Molecular Physics **52**, 255–268 (1984).
- [7] S. Nosé, *A Unified Formulation of the Constant Temperature Molecular Dynamics Methods*, Journal of Chemical Physics **81**, 511–519 (1984).
- [8] W.G. Hoover, *Canonical Dynamics: Equilibrium Phase-Space Distributions*, Physical Review A **31**, 1695–1697 (1985).
- [9] H.A. Posch, W.G. Hoover, F.J. Vesely, *Canonical Dynamics of the Nosé Oscillator: Stability, Order, and Chaos*, Physical Review A **33**, 4253–4265 (1986).
- [10] W.G. Hoover, B. Moran, *Phase-Space Singularities in Atomistic Planar Diffusive Flow*, Physical Review A **40**, 5319–5326 (1989).
- [11] E. Ott, W.D. Withers, J.A. Yorke, *Is the Dimension of Chaotic Attractors Invariant Under Coordinate Changes?*, The Journal of Statistical Physics **36**, 687–697 (1984).

- [12] T. Tél, M. Gruiz, *Chaotic Dynamics; An Introduction Based on Classical Mechanics*, Cambridge University Press (2006).
- [13] J.L. Kaplan, J.A. Yorke, *Chaotic Behavior of Multidimensional Difference Equations*, [In:] *Functional Differential Equations and the Approximation of Fixed Points*, Eds. H.O. Peitgen, H.O. Walther, Springer, Berlin, 204–227 (1979).
- [14] T. Tél, P. Gaspard, G. Nicolis, *Chaos and Irreversibility: Introductory Comments*, *Chaos* **8**, 309 (1988).
- [15] R.J. Fox, *Construction of the Jordan Basis for the Baker Map*, *Chaos* **7**, 254–269 (1997).
- [16] J. Kumičák, *Irreversibility in a Simple Reversible Model*, *Physical Review E* **71**, 016115 (2005).
- [17] W.G. Hoover, C.G. Hoover, F. Grond, *Phase-Space Growth Rates, Local Lyapunov Spectra, and Symmetry Breaking for Time-Reversible Dissipative Oscillators*, *Communications in Nonlinear Science and Numerical Simulation* **13**, 1180–1193 (2006).
- [18] W.G. Hoover, *Compressible Baker Maps and Their Inverses. A Memoir for Francis Hayin Ree [1936–2020]*, *Computational Methods in Science and Technology* **26**, 5–13 (2020).
- [19] J.D. Farmer, *Information Dimension and the Probabilistic Structure of Chaos*, *Zeitschrift für Naturforschung* **3A**, 1304–1325 (1982).
- [20] S. Tasaki, T. Gilbert, J.R. Dorfman, *An Analytical Construction of the SRB Measures for Baker-Type Maps*, *Chaos* **8**, 424–443 (1998). Note Fig. 4.



Bill and Carol Hoover moved from California to Nevada in 2005, attracted by the lack of crowding, pollution, and state income tax. Through the internet they have been able to continue research collaborations with colleagues world wide. Bill did his graduate degrees work at the University of Michigan (1960–1962) with MSChem and PhD degrees in Chemical Physics. Carol did her graduate PhD (1975–1978) work in Plasma Physics while a Student Employee at the Lawrence Livermore Laboratory and the University of California at Davis, where Bill was a member of her Doctoral Committee. They married in 1988, prior to their sabbatical year in Yokohama, working with Professors Boku, Nosé, Kawai, all at Keio University/Yokohama, and Sergio Ihara (Hitachi, Kokobungi, Japan). They have authored eight books and about 300 publications through the years with the most recent book, *Elegant Simulations; From Simple Oscillators to Many-Body Systems* coauthored by Clint Sprott (Madison, Wisconsin) published by World Scientific in early 2023. The Hoovers have continued their research, emphasizing simple models linked to macroscopic systems in Ruby Valley Nevada, where the main activity is raising thousands of Angus cattle in a close-knit mountain valley of about 200 residents. Bill's first two books, *Molecular Dynamics* (Springer-Verlag, 1986) and *Computational Statistical Mechanics* (Elsevier, 1991), are excellent introductions to their subjects.